J Mater Sci (2021) 56:17994–18005

Ceramics

Pressure-assisted direct bonding of copper to silicon nitride for high thermal conductivity and strong interfacial bonding strength

Jiabin Hu[1], Yajing Wu[1], Cong Li[1], Laili Wang[2], Shenghe Wang[3], and Zhongqi Shi[1,*]

[1] State Key Laboratory for Mechanical Behavior of Materials, Xi'an Jiaotong University, Xi'an 710049, China
[2] School of Electrical Engineering, Xi'an Jiaotong University, Xi'an 710049, China
[3] State Grid Anhui Electric Power Co., Ltd, Hefei 230061, Anhui, China

Received: 7 June 2021
Accepted: 7 September 2021
Published online: 18 September 2021

ABSTRACT

To achieve superior thermal and mechanical properties of copper-bonded (Cu-bonded) Si_3N_4 substrate, a pressure-assisted direct bonded Cu (DBC) technique was applied to bond Cu foil with Si_3N_4 plate. The effects of oxide layer (SiO_2) thickness of Si_3N_4 plate on the microstructure, thermal and mechanical properties of the Si_3N_4-DBC samples were investigated. The successful bonding of Cu foil to Si_3N_4 plate was confirmed by the presence of the interfacial products of Cu_2MgSiO_4 and $CuYO_2$. Additionally, it was demonstrated that a thin SiO_2 layer can result in a discontinuous distribution of interfacial products while a thick one can lead to the formation of pores in SiO_2 layer. Notably, the sample prepared by Si_3N_4 plate with 5-μm-thickness SiO_2 layer and Cu foil with 5.9-μm-thickness oxide layer (Cu_2O) exhibited the optimally comprehensive properties with thermal conductivity of 92 $W{\cdot}m^{-1}{\cdot}K^{-1}$ and shearing strength of 102 MPa, which demonstrates significant promise for application in power electronic modules.

Handling Editor: David Cann.

Address correspondence to E-mail: zhongqishi@mail.xjtu.edu.cn

https://doi.org/10.1007/s10853-021-06521-w

GRAPHICAL ABSTRACT

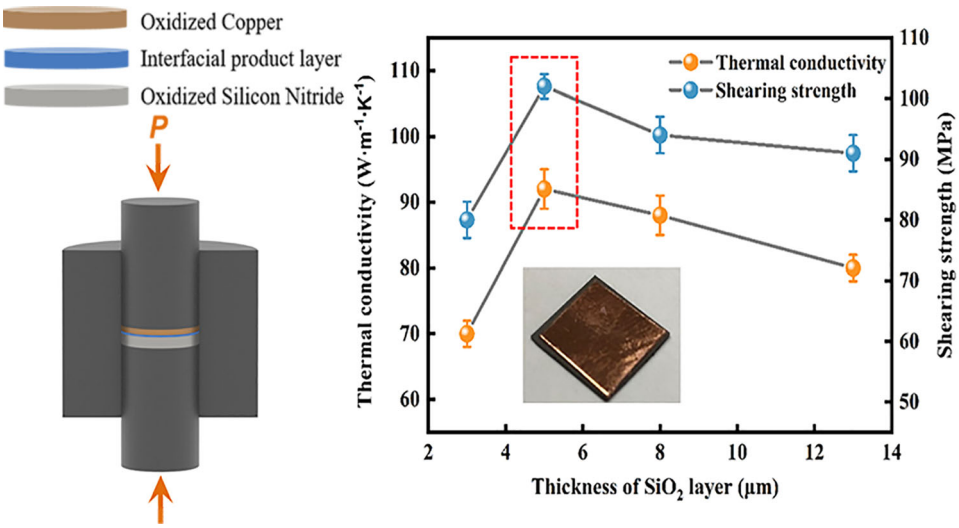

Introduction

Owing to the development of power devices toward miniaturization and high integrity, the current density within the devices rises rapidly, resulting in a large amount of heat generated during working [1–3]. Heat accumulation may cause the formation of hot spots within the microelectronic devices, and probably brings about thermal failures. Hence, the electronic substrates with reliable mechanical properties and excellent thermal conductivity need to be explored.

Direct bonded copper (DBC) substrates have made an excellent contribution to the packaging of power electronics over the last decades [4], which possess the merits of high current carrying capability, high thermal conductivity, low coefficient of thermal expansion matching with semiconductors (such as Si, SiC, etc.) and excellent electrical isolation. Therefore, DBC substrates have been used in the field of high-power devices including insulated gate bipolar translator (IGBT) modules and light-emitting diodes (LEDs) [5]. The DBC substrate is a ceramic plate bonded with Cu at one or two sides. After pre-oxidation of the ceramic plate and Cu foil, they can be bonded directly by a glass-phase interfacial layer of several microns in thickness [6]. The wettability between ceramic and Cu is considerably enhanced via the formation of Cu–O eutectic liquidoid above the eutectic point of 1065 °C [7]. This technique has been widely applied in the preparation of Al_2O_3-DBC [4, 5, 7, 8] and AlN-DBC [6, 9–11] substrates.

Compared with the above substrates, the Si_3N_4-DBC substrate has aroused great attention recently due to its high thermal conductivity and reliable mechanical properties. These advantages are attributed to the excellent properties of Si_3N_4 ceramics, including high theoretical thermal conductivity (a-axis: 170 $W{\cdot}m^{-1}{\cdot}K^{-1}$; c-axis: 450 $W{\cdot}m^{-1}{\cdot}K^{-1}$) [12, 13], superior flexural strength (usually > 500 MPa) [14–18], similar thermal expansion coefficient ($\sim 3.2 \times 10^{-6}\ K^{-1}$) [19] with that of silicon ($\sim 2.6\ K^{-1}$) [20] and excellent electrical insulating performance. Kim et al. [21] realized the direct bonding of Cu to 5 wt.% MgO-doped Si_3N_4 plate but a relatively weak shearing strength of 10.6 MPa was obtained. The low shearing strength mainly results from the pores in the interfacial oxide layer. Later, progress has been made by Tanaka et al. [22] that the Si_3N_4-DBC substrate with high interfacial bonding strength of 90–100 MPa was fabricated via the

pressure-less bonding of Cu to oxidized Si_3N_4 between 1075 and 1080 °C for 10 min in inert gas, but the thermal conductivity of only 20 $W{\cdot}m^{-1}{\cdot}K^{-1}$ for Si_3N_4 plates was not quite satisfying. Therefore, it is urgent to develop a novel route for the fabrication of Si_3N_4-DBC substrates with high thermal conductivity and good interfacial bonding strength.

It is well known that the Si_3N_4 plate can be wet by the eutectic phase Cu–O in the DBC process to insure the bonding between the ceramic plate and the Cu foil, with oxygen being introduced in the form of oxide layers. Thus, the adequate oxide layer is beneficial to the bonding between Si_3N_4 and Cu. However, after the realization of the bonding of Cu to Si_3N_4, a thick oxide layer would act as thermal barrier and would also lead to pore formation. This could deteriorate the thermal and mechanical performance of the Si_3N_4-DBC substrate. Consequently, it is important to obtain the oxide layer with proper thickness to both ensure a good connection and avert pore formation. Up to now, the most reported literature [23–25] focused on the pressure-less preparation of ceramic-DBC substrates while little attention was paid to the pressure-assisted direct bonding of Cu to ceramic plates. Spark plasma sintering (SPS) is an effective hot-pressing method where the sample can be heated at a very rapid heating rate through Joule-heating and simultaneously loaded with axial pressure [26–29]. On one hand, sparking among substances can improve the heat conductance and the diffusion of atoms at the bonding interface; on the other hand, the axial pressure applied for benefits the close contact between Si_3N_4 plates and Cu foils, and ensures the good spreading of liquid eutectic liquidoid on Si_3N_4 plates [30, 31]. The two features both can contribute to the bonding of Cu to ceramic plates and thus be expected to improve the thermal and mechanical properties of Si_3N_4-DBC substrate simultaneously.

Herein, a novel pressure-assisted DBC method was proposed to prepare the Si_3N_4-DBC substrates with both high thermal conductivity and good interfacial bonding strength. The effects of SiO_2 layer thickness of Si_3N_4 plate on the microstructure, thermal and mechanical properties of the Si_3N_4-DBC samples were investigated. In addition, the bonding process of Cu to Si_3N_4 was discussed.

Materials and methods

Raw materials

Si_3N_4 plate was fabricated in an SPS furnace (Ed-PASIII, Elenix Ltd., Japan). Si_3N_4 powder (Ube Industries Ltd., Japan, E-10 Grade) was used as raw material, and MgO powder (Shanghai Chaowei Nano Technology Co. Ltd., China, purity > 99.9%) and Y_2O_3 powder (Shanghai Chaowei Nano Technology Co. Ltd., China, purity > 99.9%) were used as sintering additives. First, Si_3N_4, MgO and Y_2O_3 powders with a molar ratio of 93:5:2 were mixed and sintered by SPS at 1700 °C holding for 5 min in a vacuum under 50 MPa, and then the dense Si_3N_4 plates were prepared. The X-ray diffraction (XRD) pattern and metallography of self-prepared Si_3N_4 plates are shown in Fig. 1a, b, respectively. In Fig. 1a, the main phase of the prepared ceramic plate is β-Si_3N_4 while the secondary phases are $Y_2Si_2O_7$ and Mg_2SiO_4. $Y_2Si_2O_7$ and Mg_2SiO_4 should be formed by the reactions between the sintering aids (Y_2O_3 and MgO) with the oxide layer (SiO_2) of Si_3N_4 powder during the sintering process. As depicted in Fig. 1b, the elongated β-Si_3N_4 grains (gray part) are closely contacted with each other while the intergranular phase (white part) locates in the triple junctions of β-Si_3N_4 grains, and few pores can be observed. The Si_3N_4 plates were machined and polished to a dimension of Φ 12.7 mm × H 2.0 mm and their surface roughness (Ra) of about 1.0 μm was obtained. Then, the obtained Si_3N_4 plates were ultrasonically cleaned and dried for the following pre-oxidation treatment. The thermal conductivity of the self-prepared Si_3N_4 plate was tested to be 75 $W{\cdot}m^{-1}{\cdot}K^{-1}$.

Oxygen-free Cu foils (Taigang Stainless Steel Co. Ltd.) with a size of Φ 12.7 mm × 0.3 mm were cut, polished, ultrasonically cleaned, and finally, dried for subsequent use. The thermal conductivity of the Cu foil was 401 $W{\cdot}m^{-1}{\cdot}K^{-1}$.

Pre-oxidation treatments

Pre-oxidation treatment of the Si_3N_4 plate was performed in an air furnace (LHT 02/17, Nabertherm, Germany) at 1300 °C under different oxidation time (30–60 min). The Cu foil was oxidized in the air in a chamber furnace (KSL-1200X-J, Kejing, China) at 270 °C for 40 min. The XRD pattern and scanning electron microscope (SEM) images of the oxidized Cu

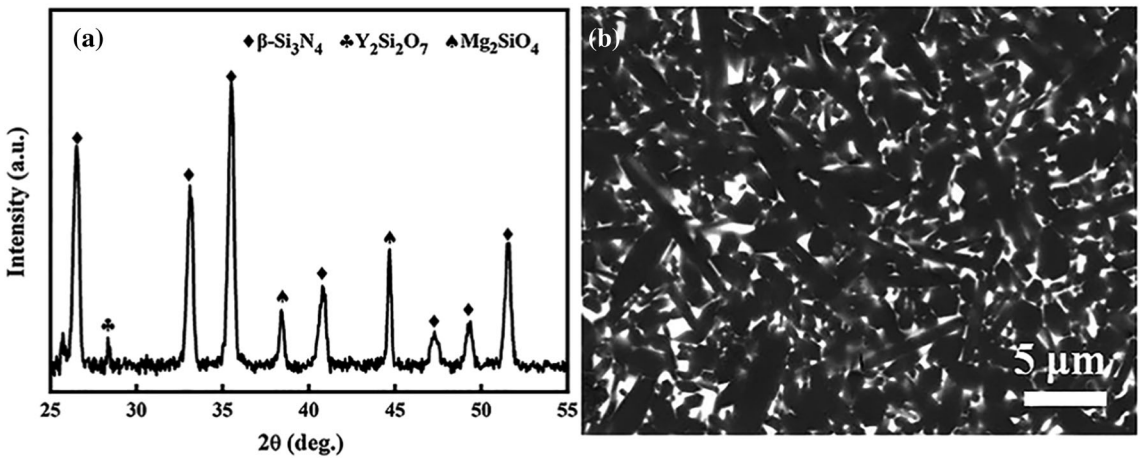

Figure 1 **a** XRD pattern and **b** metallography of self-prepared Si_3N_4 plate.

foil are provided in Supplementary Information (SI, Fig. S1 and S2). The peaks for Cu_2O are present (Fig. S1), and the Cu foil is covered with a relatively compact Cu_2O layer with a thickness of ~ 5.9 μm (Fig. S2). The thickness of the oxide layer was calculated according to the average weight gain per unit area of Si_3N_4 plate or Cu foil during the oxidation process, which can be confirmed by their cross-sectional SEM images. Each pre-oxidation process was repeated three times to ensure accuracy.

Bonding process

The Si_3N_4-DBC samples were prepared by the pressure-assisted DBC method. First, the oxidized Cu foil was placed onto the oxidized Si_3N_4 plate and both were loaded into a graphite die. Second, the sample was heated to 1075 °C in a vacuum with a holding time of 5 min under 50 MPa and then cooled down to room temperature in the furnace. To explore the effect of SiO_2 layer thickness of Si_3N_4 plate on the thermal and mechanical properties of the Si_3N_4-DBC samples, samples were fabricated by the Si_3N_4 plates with various thicknesses of the SiO_2 layer.

Characterization

The phase composition of the samples was characterized by XRD instrument (X-Pert Pro, Netherlands), and semi-quantitative analyses using X'pert HighScore Plus software were applied to analyze the phase composition and corresponding content. The microstructure and element distribution of the specimens were examined by SEM (SU3500, Hitachi,

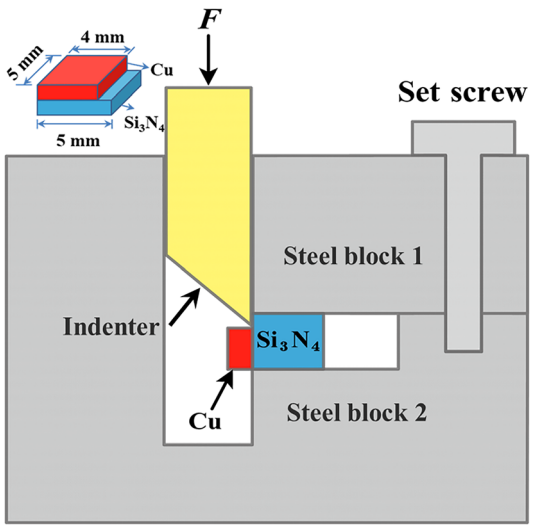

Figure 2 Schematic of shearing test for Si_3N_4-DBC samples.

Japan) equipped with the energy dispersive spectrometer (EDS). The interfacial bonding strength was tested by the electronic universal testing machine (CMT-300, Liangong, China) with a loading rate of 0.5 mm•min^{-1}. The required size of Si_3N_4-DBC samples used for the bonding strength test is shown in Fig. 2. The as-prepared Si_3N_4 plate was first cut to obtain a dimension of 5 mm × 5 mm × 2 mm, and then ground with 600-mesh, 800-mesh, 1200-mesh, 1500-mesh, and 2000-mesh abrasive disks in sequence, and finally, polished using a diamond polishing agent with an average grain size of 0.5 μm. The Cu foil was first cut into a size of 5 mm × 4 mm × 0.2 mm, and finally, ground with 1500-mesh and 2000-mesh abrasive papers. After pre-oxidation treatment, the oxidized Cu foil was bonded to the

oxidized Si_3N_4 plate via pressure-assisted DBC technology. The sample was placed in the steel mold where the ceramic plate was tightly fixed between the two steel blocks while the Cu foil was placed toward the indenter. The height difference between the Cu foil and Si_3N_4 plate helps the indenter locate at the Cu/Si_3N_4 interface to ensure the accuracy of the results. The maximum load was recorded by the electronic universal testing machine during the peeling of Cu foil from the Si_3N_4 plate. The shearing strength was calculated on the basis of the formula:

$$\sigma_s = F_s/(b \cdot h) \quad (1)$$

where σ_s, F_s, b and h represent the shearing strength (MPa), maximum load (N), width (mm), and height (mm) of the bonding area, respectively. The final value of σ_s was derived from the average of the three samples. The laser flash-light method was used to measure the thermal diffusivity (α) and the specific heat capacity (C_p) of the assemblies with the Netzsch LFA447 NanoFlash at room temperature. The thermal conductivity (κ) of the substrates was calculated according to the formula: $\kappa = \rho C p \alpha$. The densities of the samples (ρ) were calculated according to the rule of mixtures, while the densities of the Si_3N_4 plate and Cu foil were obtained by the Archimedes method. Each sample was tested three times and the κ value was attained from the average of the three results.

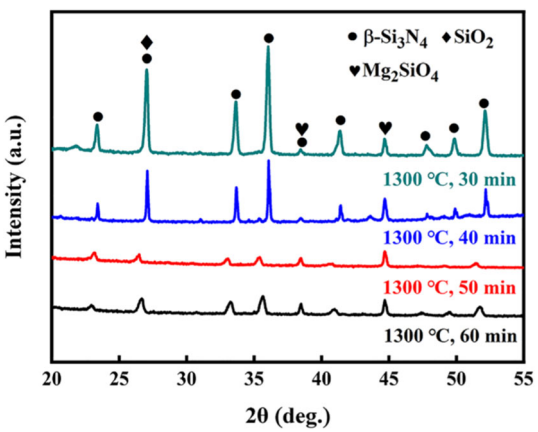

Figure 3 XRD patterns of Si_3N_4 plates oxidized at 1300 °C under different pre-oxidation time.

Results and discussion

Pre-oxidation of Si_3N_4 plates

The XRD patterns of Si_3N_4 plates oxidized at 1300 °C under different pre-oxidation time are shown in Fig. 3. Compared with Fig. 1, the Mg_2SiO_4 phase still exists while the $Y_2Si_2O_7$ phase is absent. This is because that the amount of Y atoms diffusing into the oxide layer is limited so that it can hardly be detected by a diffractometer (see Fig. S3). Besides, the SiO_2 phase can be clearly observed, which is ascribed to the oxidation of Si_3N_4 during the pre-oxidation process. In addition, the β-Si_3N_4 peak intensity decreases as the pre-oxidation time increases, which could be ascribed to the thickening of SiO_2 layer with low crystallinity.

Figure 4 shows the top and side views of the Si_3N_4 plates oxidized at 1300 °C under different oxidation time. From Fig. 4a–d, it can be noticed that the surface of Si_3N_4 plates gets rougher with oxidation time rising and flake-like grains begin to separate out at the surface when the oxidation time prolongs to 50 min (Fig. 4c). Further increasing the oxidation time to 60 min, the surface was mainly covered with sheet-shaped grains (Fig. 4d). According to the EDS results of Si_3N_4 plate oxidized for 50 min (see Fig. S3), the precipitated phase is very likely to be Mg_2SiO_4. From Fig. 4e–h, the thickness of SiO_2 layer (orange dotted line) reaches 3 μm, 5 μm, 8 μm, and 13 μm when the oxidation time is 30 min, 40 min, 50 min, and 60 min, respectively. It indicates that the thickness of SiO_2 layer can be well controlled by the oxidation time. The presence of SiO_2 can be further proved by the EDS results of the oxidized Si_3N_4 surface shown in Fig. S4. Additionally, it is worth noting that pores are formed in the SiO_2 layer when the oxidation time is not shorter than 50 min (Fig. 4g, h). This is because that the SiO_2 layer is too thick for the byproduct N_2 to escape from it timely when oxygen reacts with Si_3N_4 at high temperature. Additionally, from Fig. 4i–l, it can be observed that the amount of Mg atoms diffusing into the SiO_2 layer increases as a function of oxidation time.

Figure 5 demonstrates the relationship between weight gain per unit area of oxidized Si_3N_4 plate and pre-oxidation time. Clearly, as the oxidation time rises, the weight gain per unit area of oxidized Si_3N_4 plate exhibits an exponential growth, which proves that the oxidation process of Si_3N_4 plate is mainly

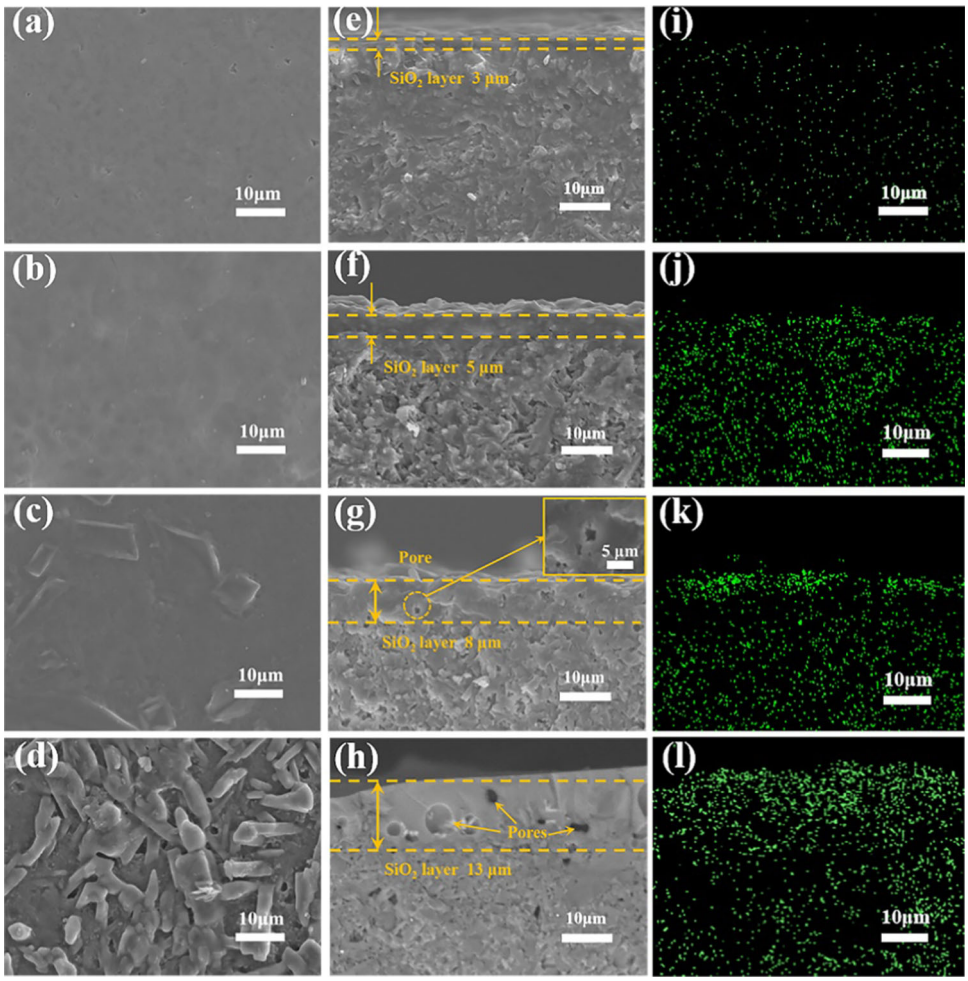

Figure 4 **a–d** Top and **e–h** side views of Si_3N_4 plates oxidized at 1300 °C under different pre-oxidation time: **a**, **e**, **i** 30 min; **b**, **f**, **j** 40 min; **c**, **g**, **k** 50 min; **d**, **h**, **l** 60 min; **i–l** Mg mappings of corresponding cross sections.

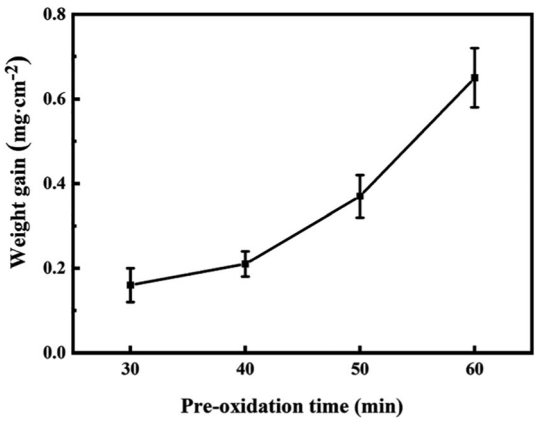

Figure 5 Weight gain per unit area of Si_3N_4 plate oxidized at 1300 °C under different pre-oxidation time.

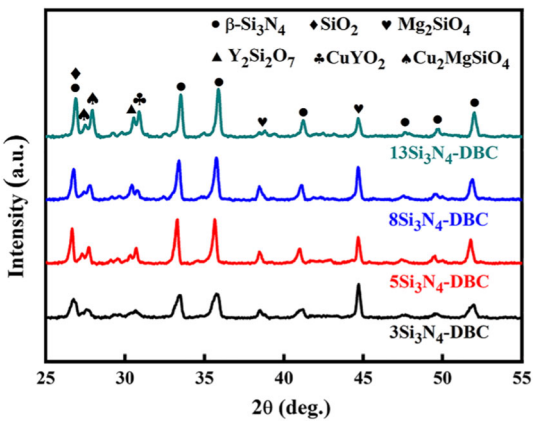

Figure 6 XRD patterns of $3Si_3N_4$-DBC, $5Si_3N_4$-DBC, $8Si_3N_4$-DBC, and $13Si_3N_4$-DBC samples after peeling of Cu foils.

dominated by surface reaction according to the Deal-Grove model [32]. Besides, the thickness of SiO_2 layer can be calculated based on the data presented in Fig. 5, and the results are basically in accord with the thicknesses marked in Fig. 4. The detailed data processing is shown in SI.

Phase composition and microstructure of Si_3N_4-DBC samples

After pre-oxidation treatment, pressure-assisted direct bonding of Cu foil to Si_3N_4 plate was conducted via hot-pressing. Samples prepared by using Si_3N_4 plates with the oxide layer thicknesses of 3 μm, 5 μm, 8 μm, and 13 μm are labeled as $3Si_3N_4$-DBC, $5Si_3N_4$-DBC, $8Si_3N_4$-DBC, and $13Si_3N_4$-DBC, respectively. Figure 6 displays the XRD patterns of the above samples. The diffraction data were collected by X-rays irradiating the newly generated interfaces of Si_3N_4 plates after peeling of Cu foils. From Fig. 6, diffraction peaks for β-Si_3N_4, SiO_2, Mg_2SiO_4, $Y_2Si_2O_7$, $CuYO_2$, and Cu_2MgSiO_4 are present in all samples. Notably, $CuYO_2$ and Cu_2MgSiO_4 emerge as interfacial products during the bonding process. The formation of $CuYO_2$ and Cu_2MgSiO_4 is probably due to the fact that Cu_2O reacts with the secondary phases $Y_2Si_2O_7$ and Mg_2SiO_4 separately. The chemical reactions could be written as follows:

$$Y_2Si_2O_7 + Cu_2O = 2CuYO_2 + 2SiO_2 \quad (2)$$

$$Mg_2SiO_4 + SiO_2 + 2Cu_2O = 2Cu_2MgSiO_4 \quad (3)$$

Due to the limited number of Y atoms diffusing into the SiO_2 layer, the amount of $CuYO_2$ derived from the reaction between $Y_2Si_2O_7$ and Cu_2O is limited. This indicates that Cu_2MgSiO_4 is the major interfacial product. Based on the semi-quantitative analyses using X'pert HighScore Plus software, the content of interfacial products in $3Si_3N_4$-DBC, $5Si_3N_4$-DBC, $8Si_3N_4$-DBC, and $13Si_3N_4$-DBC samples takes up about 2%, 5%, 6%, and 6%, respectively. As the thickness of SiO_2 layer increases, the content of interfacial products first rises from 2% and then tends to stabilize at 6%. This is mainly because the content of Cu_2O changes from excess to insufficiency compared with the total content of Mg_2SiO_4 and $Y_2Si_2O_7$ when the thickness of SiO_2 layer increases from 3 to 13 μm.

Figure 7a depicts the backscattered image of the side view of the polished $5Si_3N_4$-DBC sample. The white represents Cu foil while the light gray stands for Si_3N_4 plate. Clearly, Cu foil is in close contact with Si_3N_4 plate. There is no obvious pore or gap existing at the interface, indicating the successful bonding of Cu foil to Si_3N_4 plate. The EDS mappings of the corresponding cross sections are shown in Fig. 7b–g. It can be seen that the O element gathers at the interface to form a brighter strip presented in Fig. 7e. This is because the oxide layers of Cu_2O and SiO_2 leading to a higher O content at the interface than at other sites. To further prove the well connection between Cu foil with Si_3N_4 plate, linear scanning of the cross section of the sample was applied for analysis. From Fig. 7h, all elements show a

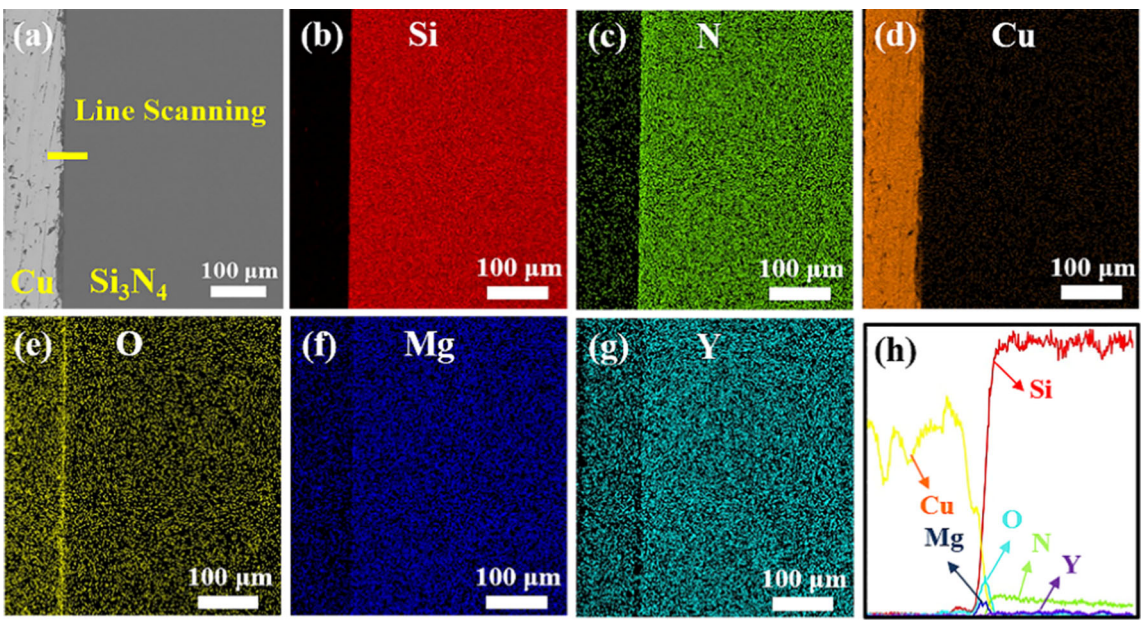

Figure 7 **a** Backscattered image of side view of polished $5Si_3N_4$-DBC sample; **b–g** EDS results of corresponding cross sections; **h** EDS linear scanning result of the cross section of $5Si_3N_4$-DBC.

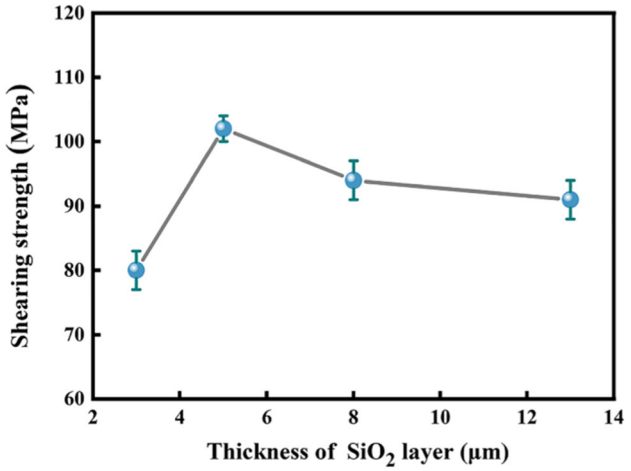

Figure 8 Interfacial shearing strength of Si_3N_4-DBC samples prepared by oxidized Si_3N_4 plates with different thicknesses of SiO_2 layer.

continuous change and no obvious step was present. Besides, in view of the results shown in Fig. 7h, the major interfacial product is considered to be Cu_2MgSiO_4, which can be further verified according to the EDS results presented in Fig. S5. All these results demonstrate a successful bonding of Cu foil to Si_3N_4 plate was realized via pressure-assisted DBC method.

Interfacial bonding strength and bonding process of Si_3N_4-DBC samples

Figure 8 depicts the interfacial shearing strength of Si_3N_4-DBC samples. Obviously, the shearing strength of Si_3N_4-DBC substrates first increases and then decreases as the thickness of SiO_2 layer arises, achieving its peak value of 102 MPa when the thickness of SiO_2 layer is 5 μm.

Figure 9 shows the fracture surfaces of Si_3N_4-DBC samples after shearing tests. From Fig. 9a, a few white particles randomly distributed on the surface of the peeled $3Si_3N_4$-DBC sample. Combined with the surface EDS mapping results (see Fig. 9b–e), the white particles are inferred to be Cu_2MgSiO_4, which is identical to the results given in Fig. 6 and Fig. S5. The isolated distribution of Cu_2MgSiO_4 reveals a lack of Cu–O eutectic liquidoid to wet the entire surface of Si_3N_4 plate, and thus a poor connection between Cu foil and Si_3N_4 plate is obtained. When the thickness of SiO_2 layer reaches 5 μm, compared with Fig. 9a–e, more Si, Mg, O and Cu elements can be observed according to the EDS results for the surface of the peeled $5Si_3N_4$-DBC sample (see Fig. 9f–j). The prolongation of pre-oxidation time from 30 to 40 min helps more Mg and Y elements diffuse into the SiO_2 layer and react with Cu_2O; hence more interfacial products are formed. This finding is basically in accord with the previous semi-quantitative analyses. Consequently, a stronger bonding of Cu to Si_3N_4 is achieved for $5Si_3N_4$-DBC samples and the highest shearing strength of 102 MPa is obtained. With the thickness of SiO_2 layer further increasing to 13 μm, some pores can be explicitly observed at the fracture surface, as indicated by the yellow arrows in Fig. 9k. The locations of pores usually result in the stress concentration, leading to the deterioration of the mechanical performance. Hence, the interfacial shearing strength of $13Si_3N_4$-DBC decreases to 91 MPa. Noticeably, from Fig. 9l, there are Si and O present at the fracture surface and their atomic ratio is close to the stoichiometric ratio of SiO_2, so the fracture is inferred to take place at the superfluous SiO_2 layer during the shearing process.

Based on the aforementioned analyses, a probable bonding process of Si_3N_4-DBC substrate is proposed, as shown in Fig. 10. The bonding process is depicted as follows:

(1) The SiO_2 and Cu_2O layers with appropriate thickness are generated at the surfaces of Si_3N_4 plate and Cu foil, respectively, after proper pre-oxidation treatments. Mg_2SiO_4 and $Y_2Si_2O_7$ are present as secondary phases in the oxide layer of Si_3N_4 plate;

(2) Cu–O eutectic liquidoid is formed at the interface between Cu foil and Si_3N_4 plate with temperature elevating above the eutectic temperature. The formation of Cu–O eutectic liquidoid can greatly reduce the contact angle of Cu to Si_3N_4. Moreover, the Cu foil is in close contact with the Si_3N_4 plate by pressure-assisted DBC method;

(3) The glass phases of Mg_2SiO_4 and $Y_2Si_2O_7$ are dissolved into the Cu–O eutectic liquidoid. When the concentration of Mg^{2+}, Y^{3+} and Si^{4+} reaches their concentration limits in the Cu–O eutectic liquidoid, Cu_2MgSiO_4 and $CuYO_2$ products would precipitate at the interface. The growth of the interfacial layer largely depends on the diffusion rates of Mg^{2+}, Y^{3+}, Si^{4+}, Cu^{2+} and O^{2-};

(4) Owing to the higher thermal conductivity of Cu foil than Si_3N_4 plate, the Cu–O eutectic

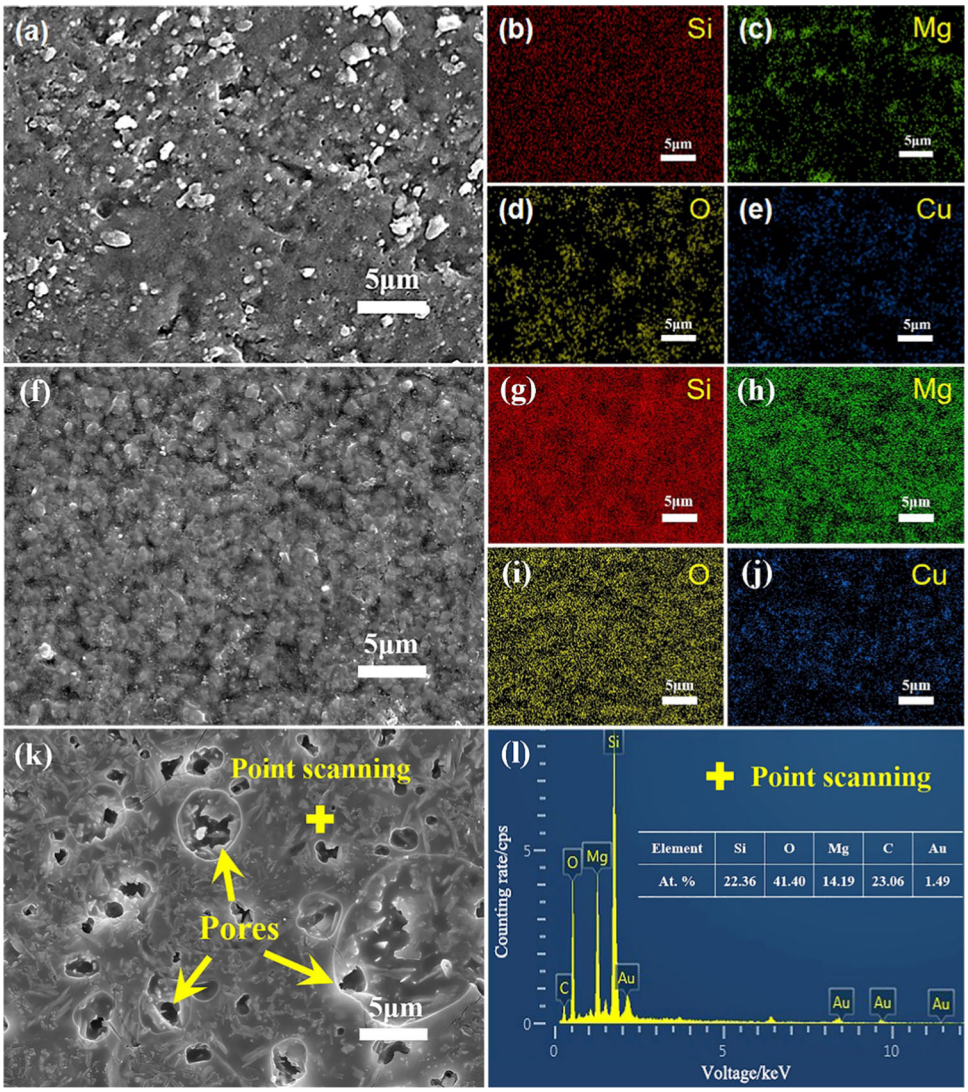

Figure 9 Morphologies of **a** $3Si_3N_4$-DBC, **f** $5Si_3N_4$-DBC, and **h** $13Si_3N_4$-DBC after peeling of Cu foils; EDS results for the fracture surfaces of **b–e** $3Si_3N_4$-DBC, **g–j** $5Si_3N_4$-DBC and **l** $13Si_3N_4$-DBC.

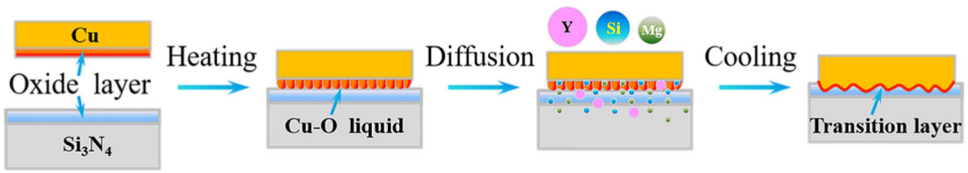

Figure 10 The principal diagram of the bonding process.

liquidoid solidifies from the side of Cu foil during the cooling process. The solidification front of Cu–O eutectic liquidoid gradually moves toward the side of Si_3N_4 plate until its meet with Si_3N_4 layer, and finally, the bonding process is accomplished.

Thermal conductivity of Si_3N_4-DBC substrates

Figure 11 depicts the thermal conductivity of Si_3N_4-DBC samples prepared by oxidized Si_3N_4 plates with different thicknesses of SiO_2 layer. The changing trend of thermal conductivity is similar with that of interfacial shearing strength, that is, it first rises and then decreases as the thickness of SiO_2 layer increases. When the thickness of SiO_2 layer rises from 3 to 5 μm, the thermal conductivity of Si_3N_4-DBC

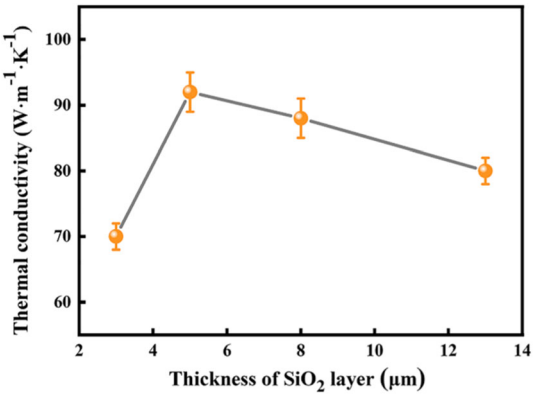

Figure 11 Thermal conductivity of Si_3N_4-DBC samples prepared by oxidized Si_3N_4 plates with different thicknesses of SiO_2 layer.

increases from 70 $W{\cdot}m^{-1}{\cdot}K^{-1}$ to its peak value of 92 $W{\cdot}m^{-1}{\cdot}K^{-1}$. Garret et al. [33] found that the thermal resistance reduces when the particle size grows in the composites. In sample $3Si_3N_4$-DBC, Cu_2MgSiO_4 precipitates distributed discontinuously at the interface as presented in Fig. 9a, contributing to a large interface thermal resistance between Si_3N_4 plate and Cu foil, thus a low thermal conductivity is obtained. In sample $5Si_3N_4$-DBC, the prolongation of pre-oxidation time from 30 to 40 min helps more Mg elements diffuse into the SiO_2 layer (see Fig. 4i–l) and react with Cu_2O. Hence, more interfacial products can be formed. This finding basically accords with the previous semi-quantitative analyses. The increase of interfacial products enhances the bonding of Cu foil to Si_3N_4 plate and the good connection between Cu foil and Si_3N_4 plate effectively reduces the interfacial thermal resistance, and thus a high thermal conductivity is achieved. However, with the SiO_2 thickness further increasing to 13 μm, the thermal conductivity falls to 80 $W{\cdot}m^{-1}{\cdot}K^{-1}$, which can be ascribed to the following two reasons. First, the size and number of pores increase when the thickness of SiO_2 layer goes up from 5 to 13 μm and pores can greatly impede the phonon and electron propagation. Second, the thermal conductivity of SiO_2 layer (27 $W{\cdot}m^{-1}{\cdot}K^{-1}$) is much lower than that of Si_3N_4 plate (75 $W{\cdot}m^{-1}{\cdot}K^{-1}$) and Cu foil (401 $W{\cdot}m^{-1}{\cdot}K^{-1}$). With the thickness of SiO_2 further increasing from 5 μm, superfluous SiO_2 acts as a thermal barrier, leading to the fall of thermal conductivity.

Based on the analysis in this section, it can be found that the content of interfacial products and the presence of pores both contribute to the shift of the bonding strength and thermal conductivity of prepared samples. Consequently, great attention should be put on seeking the proper thickness of SiO_2 layer, neither too thin to result in scarcity of interfacial products nor too thick to lead to pore formation, which both exert baleful effects on the thermal and mechanical performance of Si_3N_4-DBC substrates.

Conclusion

In summary, Si_3N_4-DBC substrates with high thermal conductivity and shearing strength were successfully prepared by the pressure-assisted direct bonding of Cu foil to Si_3N_4 plate. After pre-oxidation of Si_3N_4 plate at 1300 °C, the SiO_2 layer is formed, and its thickness increases with the oxidation time. The oxide layers of Si_3N_4 plate and Cu foil introduce oxygen to promote the wettability between Si_3N_4 and Cu. During the pressure-assisted DBC process, the interfacial products of Cu_2MgSiO_4 and $CuYO_2$ are formed, which bond the Cu foil to Si_3N_4 plate effectively. When the thicknesses of SiO_2 and Cu_2O layers are 5 μm and 5.9 μm, respectively, the sufficient interfacial products and the absence of pores ensure the high bonding strength and the low interfacial thermal contact resistance. Consequently, the $5Si_3N_4$-DBC samples possess the optimal comprehensive properties with thermal conductivity of 92 $W{\cdot}m^{-1}{\cdot}K^{-1}$ and shearing strength of 102 MPa. The Si_3N_4-DBC substrate prepared by the pressure-assisted DBC method can be used as a promising material in the field of high-power electronic packaging.

Acknowledgements

This work was supported by the National Key Research and Development Program of China (2017YFB0310400), the National Natural Science Foundation of China (51872222) and the Research on multi-chip parallel current sharing technology of power electronic devices based on electric-thermal optimization (SGAH0000KJJS1900437).

Supplementary Information: The online version contains supplementary material available at https://doi.org/10.1007/s10853-021-06521-w.

References

[1] Yin S, Tseng KJ, Zhao JY (2013) Design of AlN-based micro-channel heat sink in direct bond copper for power electronics packaging. Appl Therm Eng 52:120–129. https://doi.org/10.1016/j.applthermaleng.2012.11.014

[2] Tuan W-H, Lee S-K (2014) Eutectic bonding of copper to ceramics for thermal dissipation applications—a review. J Eur Ceram Soc 34:4117–4130. https://doi.org/10.1016/j.jeurceramsoc.2014.07.011

[3] Huang D, Liu Z, Harris J, Diao XG, Liu GH (2019) High thermal conductive AlN substrate for heat dissipation in high-power LEDs. Ceram Int 45:1412–1415. https://doi.org/10.1016/j.ceramint.2018.09.171

[4] Yoshino Y, Ohtsu H (1991) Interface structure and bond strength of copper-bonded alumina substrates. J Am Ceram Soc 74:2184–2188. https://doi.org/10.1111/j.1151-2916.1991.tb08281.x

[5] Lee S-K, Tuan W-H, Wu Y-Y, Shih S-J (2013) Microstructure-thermal properties of Cu/Al_2O_3 bilayer prepared by direct bonding. J Eur Ceram Soc 33:277–285. https://doi.org/10.1016/j.jeurceramsoc.2012.09.015

[6] Entezarian M, Drew RAL (1996) Direct bonding of copper to aluminum nitride. Mater Sci Eng A 212:206–212. https://doi.org/10.1016/0921-5093(96)10190-8

[7] Yoshino Y (1989) Role of oxygen in bonding copper to alumina. J Am Ceram Soc 72:1322–1327. https://doi.org/10.1111/j.1151-2916.1989.tb07645.x

[8] Yoshino Y, Shibata T (1992) Structure and bond strength of a copper-alumina interface. J Am Ceram Soc 75:2756–2760. https://doi.org/10.1111/j.1151-2916.1992.tb05500.x

[9] Kara-Slimane A, Juve D, Leblond E, Treheux D (2000) Joining of AlN with metals and alloys. J Eur Ceram Soc 20:1829–1836. https://doi.org/10.1016/S0955-2219(00)00037-6

[10] Jarrige J, Joyeux T, Lecompte JP, Labbe JC (2007) Comparison between two processes using oxygen in the Cu/AlN bonding. J Eur Ceram Soc 27:855–860. https://doi.org/10.1016/j.jeurceramsoc.2006.04.037

[11] Kluge-Weiss P, Gobrecht J (1984) Directly bonded copper metallization of AlN substrates for power hybrids. MRS Online Proc Libr 40:399–404. https://doi.org/10.1557/PROC-40-399

[12] Hirosaki N, Ogata S, Kocer C, Kitagawa H, Nakamura Y (2002) Molecular dynamics calculation of the ideal thermal conductivity of single-crystal α- and β-Si_3N_4. Phys Rev B 65:1–11. https://doi.org/10.1103/PhysRevB.65.134110

[13] Tunckan O, Yurdakul H, Turan S (2019) Unveiling the reaction products in heat treated Si_3N_4-Ti joined ceramics by transmission electron microscopy. J Adv Ceram 8:500–508. https://doi.org/10.1007/s40145-019-0330-8

[14] Tsuge A, Nishida K, Komatsu M (1975) Effect of crystallizing the grain-boundary glass phase on the high-temperature strength of hot-pressed Si_3N_4 containing Y_2O_3. J Am Ceram Soc 58:323–326. https://doi.org/10.1111/j.1151-2916.1975.tb11488.x

[15] Kovar D, Thouless MD, Halloran JW (1998) Crack deflection and propagation in layered silicon nitride/boron nitride ceramics. J Am Ceram Soc 81:1004–1012. https://doi.org/10.1111/j.1151-2916.1998.tb02438.x

[16] Hirao K, Brito ME, Toriyama M, Kanzaki S (2000) Further improvement in mechanical properties of highly anisotropic silicon nitride ceramics. J Am Ceram Soc 83:495–500. https://doi.org/10.1111/j.1151-2916.2000.tb01223.x

[17] Riley FL (2000) Silicon nitride and related materials. J Am Ceram Soc 83:245–265. https://doi.org/10.1111/j.1151-2916.2000.tb01182.x

[18] Liu SC, Ye F, Hu SQ, Yang HX, Liu Q, Zhang B (2015) A new way of fabricating Si_3N_4 ceramics by aqueous tape casting and gas pressure sintering. J Alloys Compd 647:686–692. https://doi.org/10.1016/j.jallcom.2015.05.134

[19] Krstic Z, Krstic VD (2012) Silicon nitride: the engineering material of the future. J Mater Sci 47:535–552. https://doi.org/10.1007/s10853-011-5942-5

[20] Watanabe H, Yamada N, Okaji M (2004) Linear thermal expansion coefficient of silicon from 293 to 1000 K. Int J Thermophys 25:221–236. https://doi.org/10.1023/B:IJOT.0000022336.83719.43

[21] Kim ST, Kim CH, Park JY, Son YB, Kim KY (1990) The direct bonding between copper and MgO-doped Si_3N_4. J Mater Sci 25:5185–5191. https://doi.org/10.1007/BF00580149

[22] Tanaka S-I (2009) Direct bonding of Cu to oxidized silicon nitride by wetting of molten Cu and Cu(O). J Mater Sci 45:2181–2187. https://doi.org/10.1007/s10853-009-3951-4

[23] Miyashiro F, Iwase N, Tsuge A, Ueno F, Nakahashi M, Takahashi T (1990) High thermal conductivity aluminum nitride ceramic substrates and packages. IEEE Trans Compon Packaging Manuf Technol 13:313–319. https://doi.org/10.1109/33.56163

[24] He H, Fu RL, Wang DL, Song XF, Jing M (2007) A new method for preparation of direct bonding copper substrate on Al_2O_3. Mater Lett 61:4131–4133. https://doi.org/10.1016/j.matlet.2007.01.036

[25] Hromadka K, Stulik J, Reboun J, Hamacek A (2014) DBC technology for low cost power electronic substrate manufacturing. Procedia Eng 69:1180–1183. https://doi.org/10.1016/j.proeng.2014.03.107

[26] Munir ZA, Quach DV (2011) Electric current activation of sintering: a review of the pulsed electric current sintering process. J Am Ceram Soc 94:1–19. https://doi.org/10.1111/j.1551-2916.2010.04210.x

[27] Guo YJ, Guo HT, Gao BX, Wang XG, Hu YB, Shi ZQ (2017) Rapid consolidation of ultrafine grained W-30 wt.% Cu composites by field assisted sintering from the sol–gel prepared nanopowders. J Alloys Compd 724:155–162. https://doi.org/10.1016/j.jallcom.2017.07.023

[28] Niu YH, Fu S, Zhang KB, Dai B, Zhang HB, Grasso S, Hu CF (2020) Synthesis, microstructure, and properties of high purity Mo_2TiAlC_2 ceramics fabricated by spark plasma sintering. J Adv Ceram 9:759–768. https://doi.org/10.1007/s40145-020-0412-7

[29] Permin DA, Boldin MS, Belyaev AV, Balabanov SS, Koshkin VA, Murashov AA, Ladenkov IV, Lantsev EA, Smetanina KE, Khamaletdinova NM (2021) IR-transparent MgO-Gd_2O_3 composite ceramics produced by self-propagating high-temperature synthesis and spark plasma sintering. J Adv Ceram 10:237–246. https://doi.org/10.1007/s40145-020-0434-1

[30] Suganuma K (1990) Recent advances in jointing technology of ceramics to metals. ISIJ Int 30:1046–1058. https://doi.org/10.2355/isijinternational.30.1046

[31] Kisiel R, Guziewicz M, Taube A, Kaminski M, Sochacki M (2020) Development of assembly techniques for connection of AlGaN/GaN/Si chips to DBC substrate. Circuit World 47:146–152. https://doi.org/10.1108/CW-12-2019-0186

[32] Deal BE, Grove AS (1965) General relationship for the thermal oxidation of silicon. J Appl Phys 36:3770–3778. https://doi.org/10.1063/1.1713945

[33] Garrett KW, Rosenberg HM (1974) The thermal conductivity of epoxy-resin/powder composite materials. J Phys D Appl Phys 7:1247–1258. https://doi.org/10.1088/0022-3727/7/9/311